Magnetohydrodynamics, Vol. 36, No. 4, 2000

SPINNING FERROFLUID MICROSCOPIC DROPLETS

E. Janiaud,[1,2] F. Elias,[1] J.-C. Bacri,[1,2] V. Cabuil,[3] and R. Perzynski[1]

We investigate experimentally the behavior of microscopic ferrofluid droplets under the effect of a rotating external magnetic field. Depending on the system control parameters, the drops adopt fascinating shapes, like starfish, rod-like or pancake shapes, co-rotating with the external field, but also creeping snakes, swirling loops, and rings. We describe these structures and classify them in a phase diagram. With simple arguments, we discuss the droplet dynamics and morphology in each phase.

Introduction

When submitted to a static external magnetic field, a magnetic fluid (MF) drop changes shape. It can split into a hexagonal lattice of smaller droplets, adopt a labyrinthine structure, become elongated, or assume more complicated shapes [1, 2]. These complex morphologies find their origin in the competition between the magnetic and interfacial energies. They have recently been reviewed in a special issue of *Magnetohydrodynamics* [3]. While these points are now relatively clear, MF behavior in a rotating magnetic field is still controversial. In a pioneering experiment, with a beaker of MF immersed in a rotating magnetic field, Moskowitz and Rosensweig observed a peculiar feature: a co-rotation flow at a frequency much lower than the frequency of the magnetic field [4]. Moreover, other experiments exhibited a counter-rotation [5, 6]. It is only recently that Rosensweig [7] and Lebedev [8] showed clearly that the macroscopic rotation of a homogeneous MF in a rotating magnetic field is due to a surface effect.

To enhance such surface effects, experiments are performed with MF microdrops made of a highly magnetic phase inside a poorly magnetic phase of a demixing ionic ferrofluid [9, 10] (for simplicity, the poorly magnetic phase will be, in the following, called nonmagnetic phase). Under the effect of a static magnetic field, the droplets stretch in the field direction. Their equilibrium shape results from the competition between the magnetic energy that tends to extend the drop along the field direction, and the surface energy which tends to minimize the MF interface. Assimilating these shapes to prolate ellipsoids, the equilibrium aspect ratio can be analytically calculated as a function of the field strength [11]. When increasing the strength of the magnetic field, a first-order transition between a slightly elongated and a strongly elongated shape is obtained [12, 13]. If the external magnetic field rotates, the droplet turns in the direction of the applied field. The viscous torque due to the friction of the drop against the nonmagnetic liquid phase is equilibrated by the magnetic torque. According to [14], and under the assumption of a rigid ellipsoidal drop (i.e., not deformed by the rotation), the equation of motion of the ellipsoid in the plane of rotation of the magnetic field is

$$\eta_0 \varepsilon \frac{\mathrm{d}\varphi}{\mathrm{d}t} = \mu_0 A \chi H_0^2 \sin[2(\omega t - \varphi)], \tag{1}$$

where

$$\varepsilon = \frac{4K^2}{2\ln(2K) - 1}, \qquad A = \frac{\chi(1-3D)}{2[2+\chi(1-D)]}.$$

[1]Laboratoire des Milieux Désordonnés et Hétérogènes, Université Paris 6, case 78, 4 place Jussieu, 75252 Paris cedex 05, France.
[2]Université Paris 7, Unité de Formation et de Recherche de Physique, case 70.08, 2 place Jussieu, 75251 Paris cedex 05, France.
[3]Laboratoire des Liquides Ioniques et des Interfaces Chagés, Université Paris 6, case 0063, 4 place Jussieu, 75252 Paris cedex 05, France.

Published in Magnitnaya Gidrodinamika, Vol. 36, No. 4, pp. 365–378, October–December, 2000. Original article submitted February 22, 2001.

 0024-998X/00/3604–0300 $ 25.00

In Eq. (1), the left term represents the viscous torque and the right term the magnetic torque. φ is the angular position of the ellipsoid long axis, H_0 and ω are respectively the amplitude and pulsation of the applied rotating magnetic field, η_0 is the viscosity of the nonmagnetic phase, χ is the magnetic susceptibility of the MF phase, K is the ellipsoid long to small axis length aspect ratio, and D is the ellipsoid demagnetizing factor depending only on K. At low frequency, Eq. (1) has a stationary solution. The ellipsoidal drop turns synchronously with the magnetic field, in a solid rotation, with a constant phase lag between its orientation and the magnetic field direction:

$$\varphi = \omega t + \frac{1}{2}\arcsin(\omega\tau_C), \qquad \text{where} \quad \tau_C = \frac{\eta_0 \varepsilon}{\mu_0 A \chi H_0^2}. \tag{2}$$

This solution exists only at low frequency, when $\omega\tau_C < 1$. The ellipsoidal drop relaxation time τ_C is typically of the order of 1 second. If $\omega\tau_C > 1$, Eq. (1) has no stationary solution. The angle $(\omega t - \varphi)$ between the drop and the magnetic field direction has to increase: the ellipsoid can no longer follow the magnetic field rotation and its motion becomes jerky. As the drop is liquid, it becomes unstable and changes shape. Several scenarios can occur. The ellipsoid can break into smaller droplets of lower aspect ratio. These secondary droplets have then a smaller relaxation time τ_C, and can rotate synchronously with the external field. This phenomenon has recently been studied in [14], where it has been showed that the droplet size and aspect ratio depend on the field frequency. The rotation and breakage of MF ellipsoids submitted to a rotating magnetic field is analogous to the motion of chains of magnetic holes in a magneto-rheologic fluid, studied in [15, 16]. When the rotating magnetic field frequency increases, the drop can assume an oblate shape crowned by spikes (starfish shape) [17, 18], which turns in the direction given by the external magnetic field rotation, but at a much lower frequency.

In this paper, we analyze the behavior of one drop as a function of the amplitude and frequency of the external rotating magnetic field in the regime $\omega > \tau_C^{-1}$. We observe prolate and oblate ellipsoids, starfish, but also more complex shapes like creeping snakes, swirling loops, or rings. We classify all the observed structures in a qualitative phase diagram. The main features of these dynamic morphologies are then interpreted in the framework of magnetohydrodynamics.

1. Experimental

We use an aqueous ionic ferrofluid, whose stability is monitored through screened electrostatic repulsion between grains. The magnetic particles are maghemite (γ–Fe_2O_3) grains, with a mean size of roughly 10 nm. In this ionic MF, a phase separation is induced, increasing the ionic strength of the solution [9, 10]. It leads to droplets of a highly concentrated phase inside a more dilute phase. Because of the low interfacial tension between the two phases, the droplets are microscopic. Their volume fraction in magnetic particles is 31% [14], whereas it is less than 0.1% for the nonconcentrated phase, which can then be considered as a nonmagnetic phase. The densities are $\rho \sim 2.5\,10^3\,\mathrm{kg\,m^{-3}}$ for the concentrated phase and $\rho_0 = 10^3\,\mathrm{kg\,m^{-3}}$ for the diluted phase. In a static external magnetic field, the MF droplets elongate in the field direction. Measurement of their equilibrium aspect ratio as a function of the field strength leads to determination of their magnetic susceptibility χ and of the interfacial tension σ [14]: $\chi = 40 \pm 10$ and $\sigma \sim 10^{-6}\,\mathrm{J\,m^{-2}}$. With such a low surface tension and high magnetic susceptibility, droplet deformation occurs for a small magnetic field (a few Gauss), which is an advantage in experiments involving rotating magnetic fields. The shape relaxation of the ellipsoidal drop when the magnetic field is switched off leads to the determination of a viscosity η of the MF concentrated phase of the order of $\eta \sim 3\,10^{-1}$ Pa·s. The viscosity of the nonmagnetic phase is equal to the viscosity of water: $\eta_0 = 10^{-3}$ Pa·s.

In the experiments, the diphasic MF is placed in a closed glass cell of 100 μm thickness, 1 cm wide, and 3 cm long. The concentrated phase does not wet the glass plates. The MF microdrops have a typical size of 10 μm. Because of their small size, they are buoyant inside the nonmagnetic phase without being deformed by gravity, as shown on Fig. 1. The cell is placed horizontally between two perpendicular pairs of coils in the Helmholtz configuration, as sketched on Fig. 2. Alternating current is supplied in phase quadrature to the two pairs of coils

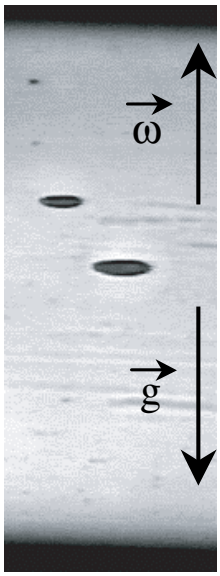

Fig. 1. Side view of two-MF drops between two glass plates. The plates appear in black at the bottom and at the top of the image. The distance between plates is 100 μm. Two black microdrops are visible in the middle of the image. They are submitted to a rotating external magnetic field in the horizontal plane (perpendicular to the plane of the figure), which spreads them out horizontally. $\boldsymbol{\omega}$ is the rotation vector of the external field, and $\boldsymbol{g}$ is the gravity. The MF drops do not wet the glass plates, but they are buoyed in the poorly magnetic liquid phase. Moreover, they are not deformed by gravity.

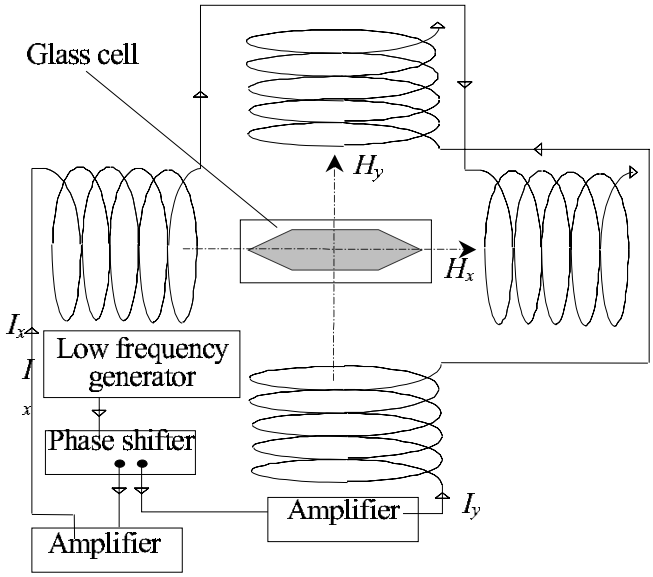

Fig. 2. Top view of the experimental set-up. The experimental glass cell, filled with the diphasic MF, is placed between two pairs of coils in the Helmholtz configuration. Each pair of coils is supplied with an alternating current in phase quadrature: $I_x = I_0 \cos(\omega t)$, $I_y = I_0 \sin(\omega t)$ in order to generate a uniform horizontal rotating magnetic field. The rotating magnetic field frequency can be varied from several Hz to several kHz. The maximum magnetic field amplitude is about 10 $\mathrm{kA\,m^{-1}}$.

to produce a uniform clockwise rotating magnetic field in the horizontal plane. The MF patterns are observed through an optical transmission microscope. The images are recorded by a CCD camera, and digitized by an acquisition card in a Macintosh computer for numerical image analysis using the NIH-Image software.

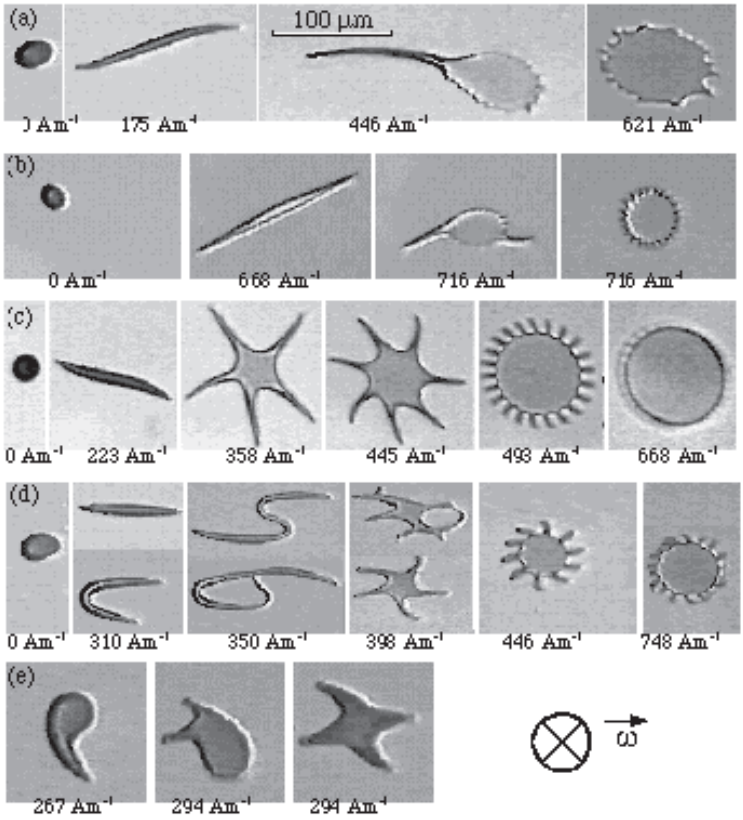

Fig. 3. MF drop submitted to a horizontal clockwise rotating magnetic field of pulsation $\omega = 2\pi f$, in the regime $\omega\tau_C >> 1$. The plane of observation is the plane of rotation of the magnetic field. (a) $f = 4$ Hz; (b) $f = 40$ Hz; (c) $f = 400$ Hz; (d) $f = 1$ kHz; (e) $f = 4$ kHz.

2. Results

The experiments are done at 5 different values of the frequency $f = \omega/2\pi$ of the rotating applied magnetic field in the regime $\omega\tau_C > 1$: $f = 4$ Hz, 40 Hz, 400 Hz, 1 kHz, and 4 kHz. In each set, f is kept constant and the field strength is increased step by step from 0 to 750 $\mathrm{A\,m^{-1}}$, waiting 10 minutes between each step for the pattern to stabilize. We describe below all the different possible shapes adopted by the MF drop and we group them in categories in order to sketch a qualitative phase diagram.

Beyond all the different drop behaviors, some general features can be extracted. The MF droplet turns always in co-rotation with the magnetic field. The drop spinning frequency is always very slow compared to the magnetic field frequency: the maximum measured value is a few Hz even with a rotating field of a few kHz.

2.1. Observed shapes. The droplet shapes obtained at a given amplitude and frequency of the magnetic field are presented in Fig. 3.

$f = 4$ Hz (Fig. 3a): starting from a spherical drop at $H_0 = 0$, one clearly sees a transition to a slender ellipsoid pointing in a random direction. The ellipsoid first elongates as H_0 increases without any rotation of the drop but only a 4 Hz tip beating. The amplitude of this beating increases up to a transition in which the drop changes to a flat spinning shape (last image), clockwise rotating at a much lower frequency (about 1 Hz) than that of the magnetic field. The picture at $H_0 = 446\,\mathrm{A\,m^{-1}}$ in Fig. 3a represents the drop in the transient regime just before it assumes a flat spiny shape. Note that the drop interface is covered by hairy spikes whose direction oscillates at the frequency of the applied field.

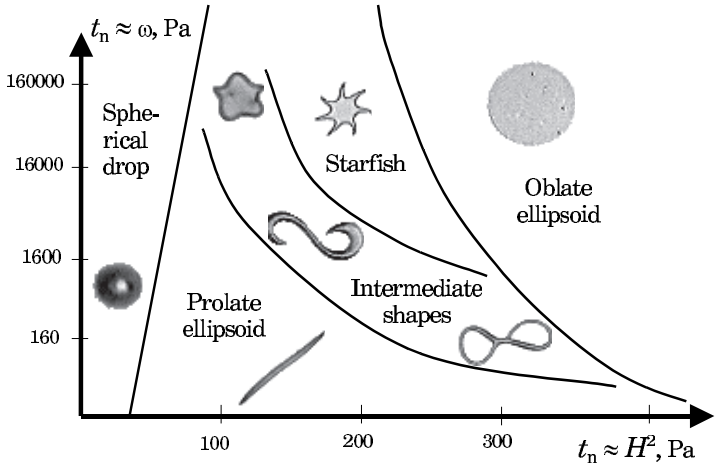

Fig. 4. Morphological phase diagram of a MF drop submitted to a rotating magnetic field of pulsation ω and amplitude H_0, as a function of the normal and tangential stresses. t_n and t_t are expressed in Eqs. (3) and (4) (see text). If the drop volume is fixed, $t_n \approx H_0^2$ and $t_t \approx \omega$. For low H_0 and whatever ω, the drop is always spherical or has a slightly oblate ellipsoidal shape. For low ω and H_0 above a threshold value, the drop shape is always a prolate ellipsoid. For high H_0 and high ω, the drop is a stable oblate ellipsoid. Starting from this latter shape and decreasing either H_0 or ω, the drop becomes a spiny starfish, then adopts a complicated morphology ("S" or a "8" shape, for instance), intermediate between the starfish and the prolate ellipsoid. These intermediate shapes are never stable and evolve constantly. The starfish and intermediate shapes do not exist for low values of ω.

$f = 40$ Hz (Fig. 3*b*): for low values of H_0, a transition from a spherical shape to a steady prolate shape is observed. When H_0 increases, this prolate slender shape flattens from the middle. The drop shape then transforms into a hairy flat shape, which spins clockwise at a low frequency.

$f = 400$ Hz (Fig. 3*c*): the transition to the prolate shape yields a slender body, not as rigidly stretched as in the two previous experiments, but gently curved and bent, rotating at a very low frequency (less than one Hertz). The larger the field, the larger the curvature. At $H_0 = 358\,\mathrm{A\,m^{-1}}$, this shape changes to a clockwise spinning starfish, with the number of spikes increasing with H_0. At $H_0 = 668\,\mathrm{A\,m^{-1}}$, spikes are hardly visible at the interface: the shape is oblate ellipsoid.

$f = 1$ kHz (Fig. 3*d*): the same shapes as for f = 400 Hz are observed. For the same value of H_0, the rotating frequency and the drop curvature are increased in comparison with the case $f = 400$ Hz.

f = 4 kHz (Fig. 3*e*): no elongated shape is observed, but only a stocky star shape with a number of arms and a spinning frequency that increases with H_0.

All the described shapes are classified in the qualitative phase diagram presented in Fig. 4. They can be grouped in 5 categories:

– for low H_0, the drop is not deformed and remains spherical;

– for low magnetic field pulsation ω and above a threshold value of H_0, the drop always assumes a prolate ellipsoid shape;

– for high values of ω and H_0, it turns into an oblate ellipsoid;

– starting from this latter phase and decreasing either H_0 or ω, the starfish shape is adopted;

– finally, unstable shapes like creeping snakes or swirling loops are observed between the prolate ellipsoid phase and the starfish phase. We describe these morphologies as intermediate shapes.

The spherical, prolate, oblate, and starfish morphologies are all stationary shapes: after a transient regime, the shape remains invariant and the drop motion is a solid rotation. On the other hand, the intermediate shapes are nonstationary: the liquid drop constantly deforms in this regime. Contrary to the case of stationary shape, the drop motion and morphology are coupled in an intricate mechanism. The transient regime of a stationary shape as well as the dynamics of intermediate forms are presented below.

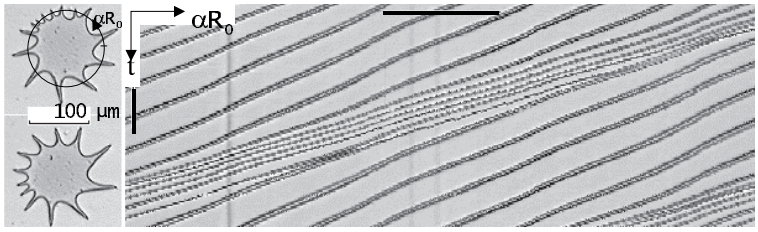

Fig. 5. Transient regime of the rotation of a MF star after changing H_0. $H_0 = 358\ \mathrm{A\,m^{-1}}$ and f = 400 Hz. On the left: images of the drop at two different times: two different wavelength are visible at the drop circumference. On the right: space-time diagram of the drop motion. The drop circumference is recorded as a function of time. The horizontal bar represents 100 μm and the vertical bar represents 1 s. Two different wavelengths are visible, as well as the difference in the rotation velocity: the peak rotation frequency in the large wavelength region is 0.19 Hz, whereas it is 0.26 Hz in the small wavelength region.

2.2. Transient regime of the MF star shape. Let us focus on the MF star shape. The number of star arms is fixed by the external parameters H_0, ω, and the droplet volume V (see Sec. 3). When one of these parameters is changed, the star adopts its new equilibrium morphology going through a peculiar transient regime. Figure 5 shows a MF drop just after H_0 is changed. At $t = 0$, the number of star arms is larger than its equilibrium value and some peaks have to disappear. In other words, the average distance between peaks is too small compared to its equilibrium value. Instead of being spread over the whole drop surface, the deformation is strong only in a small portion of the drop, which has a smaller wavelength and a smaller amplitude than the rest of the surface. During the drop rotation, the deformation turns faster than the undeformed region of the interface, in the same direction: new peaks join the deformation at its head, whereas peaks leave the deformation at its tail. Nevertheless, peaks lose matter during the propagation of the deformation and end up coalescing with another peak. This progressively decreases the total number of spikes and the drop can reach its equilibrium shape. A space-time diagram of the drop circumference is shown in Fig. 5: the difference in spike velocities and wavelength appear clearly. This transient regime is long compared to the other characteristic times in the problem: it takes several minutes for a drop to achieve its equilibrium shape when one of the control parameters is changed.

2.3. Intermediate nonstationary shapes. The intermediate shapes between the ellipsoidal drop phase and the starfish shape presented in the phase diagram (Fig. 4) are dynamic and unstable. Starting from the prolate ellipsoid phase and increasing either H_0 or ω, the drop bends at the ends and adopts an "S" shape, as shown in Figs. 6a and 7a. This structure is not stable and the drop shape transforms into more complicated morphologies. Several scenarios can occur.

The drop ends can go into circular motion and coalesce in the middle of the drop, forming an "8" shape (Fig. 6b). The "8" shape involves an important curvature and is usually not stable. The drop then breaks in the region where the curvature is the most important.

In Fig. 6c, the drop breakage leads to the formation of spikes, which turn with the drop. From Fig. 6c to Fig. 6f, the morphology is constantly alternating between the "S" shape and the starfish shape.

Starting from the "S" shape, the ellipsoid can also spin around itself at its ends (Fig. 6g and 6h). The flat part of the drop then tends to form spikes at its interface. Here again, the drop does not stabilize in a steady shape but seems to hesitate between the ellipsoidal shape and the star shape.

In Fig. 7b, the drop breaks into three droplets, corresponding to the three unbent parts of the "S" shape. These three ellipsoidal droplets then turn in the same direction as the field, with a frequency that depends on their volume: the smaller the drop, the higher its spinning frequency. After several rotations, the droplets coalesce to reform the initial "S" shape (Fig. 7i). This complex breakage–spinning–coalescence motion occurs with a periodicity of the order of 22 seconds. It is analogous to the quasiperiodic motion of chains of magnetic holes inside a MF, submitted to a rotating magnetic field [15].

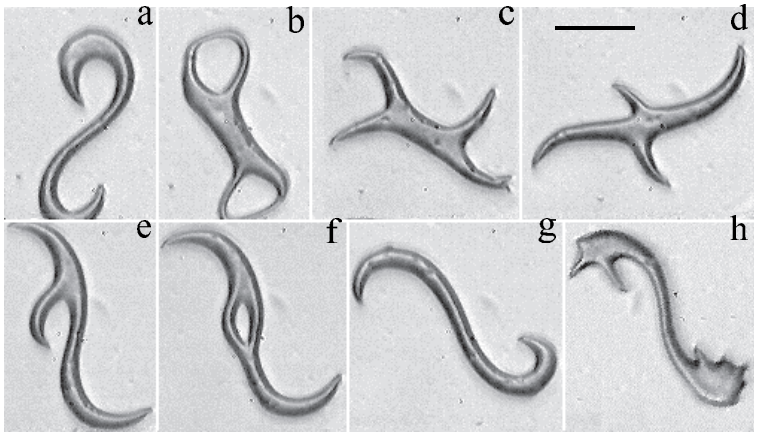

Fig. 6. Ferrofluid drop in the intermediate regime. $H_0 = 220\,\mathrm{A\,m^{-1}}$ and f = 400 Hz. (a) t = 0, (b) t = 5 s, (c) t = 7 s, (d) t = 10 s, (e) t = 13 s, (f) t = 17 s, (g) t = 18 s, (h) t = 21 s, (i) t = 26 s.

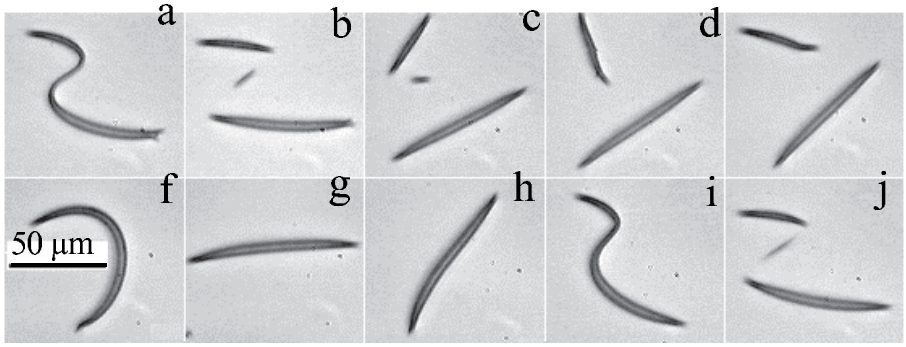

Fig. 7. Ferrofluid drop in the intermediate regime: breakage, rotation and coalescence with a fixed periodicity. $H_0 = 316\,\mathrm{A\,m^{-1}}$ and f = 40 Hz. (a) t = 0, (b) t = 0.3 s, (c) t = 3.6 s, (d) t = 4.4 s, (e) t = 5.4 s, (f) t = 8.4 s, (g) t = 11.9 s, (h) t = 17.4 s, (i) t = 21.5 s, (j) t = 22.6 s.

3. Discussion

Obviously, a full understanding of the observed pictures is beyond the scope of this paper, but let us focus on some salient features which can be understood from the microscopic aspect of a MF in a rotating field.

3.1. Why do the drops spin? A surface effect. At the microscopic level, the colloid MF is made up of an assembly of rigid magnetic dipoles, which spin at the frequency of the external magnetic field (their Brownian relaxation time is of the order of 0.1 ms, smaller than the period of the rotating magnetic field). There is a constant phase lag between the external field direction and the magnetic momentum of the particles, due to the viscous friction against the carrier liquid, equilibrated by the magnetic torque. Inside the MF drop, the corotation of two neighboring particles is dissipated by viscous friction; only at the interface is the friction low and the MF interface can rotate (see on Fig. 8). After a transient regime, the whole MF volume is involved in a solid rotation.[4] Depending on the sign of curvature of the interface, the motion can be a corotation or a counter-rotation, as sketched on Fig. 8. In our experiments, the MF drops are convex and therefore always in corotation with the field (in the case of a droplet of nonmagnetic phase inside the magnetic phase, a counter-rotation is observed [19]).

[4]Some dusts present inside the MF drop indicate that the drop spinning motion is a rigid rotation.

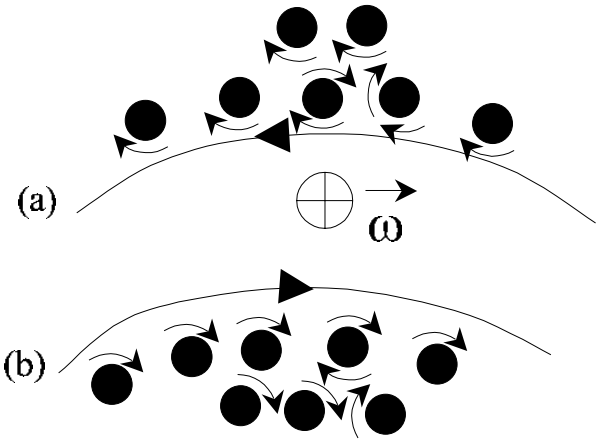

Fig. 8. Rotation of a MF interface due to the rotation of the magnetic particles inside the MF phase. $\boldsymbol{\omega}$ is the rotation vector of the external magnetic field. The black spots represent the magnetic particles, which turn at the same pulsation $\boldsymbol{\omega}$ as the field. (a) In the case of a concave interface, a counter-rotation of the interface with respect to the field is obtained. (b) In the convex case, the interface is in co-rotation with the field.

Macroscopic experiments presented in [7] and [8] are in agreement with this simple argument.

From a macroscopic point of view, the interface motion is due to an asymmetric viscous stress tensor. The stress experienced by a surface element of the interface can be split into two components: a normal stress and a tangential stress, as sketched in Fig. 9. The normal stress has only a magnetic contribution [7]:

$$t_n = \frac{1}{2}\mu_0 M_n^2, \tag{3}$$

where M_n is the mean normal component of the MF magnetization. The tangential component of the stress tensor is due to the viscous drag of the spinning magnetic particles that is not equilibrated near the interface. If the frequency of the magnetic field is larger than that of the droplet rotation (which is experimentally always the case in the regime of studied frequencies), the tangential stress can be written as [7]:

$$t_t = 2\xi\omega \sin\beta, \tag{4}$$

where ξ is the MF rotational viscosity [20] and β is the angle between the normal to the surface and the magnetic field rotation vector $\boldsymbol{\omega}$.

Equations (3) and (4) provide us with a simple interpretation of our experiments: the normal stress experienced by the interface tends to spread out radially the drop in the plane of rotation of the magnetic field. From Eq. (3), the drop shape can therefore be described. Equation (4) explains the drop rotation motion: the tangential stress, acting as a torque, yields to a corotation of the drop with the field; the larger the frequency, the larger the rotational effect compared to the radial one.[5] The tangential stress intensity does not depend on the particular geometry of the droplet (contrary to the normal stress intensity that is a function of the local orientation of the interface): shape and rotation motion of the MF drop are therefore decoupled. Indeed, Fig. 3*c*, 3*d* and 3*e* show that in the case of a rotating MF star, the spikes are bent in the direction opposite to the drop rotation. The spikes resist the motion instead of being a motor for the drop rotation, as would be expected if shape and motion were coupled. Let us note that this simple interpretation is valid only in the case of stationary shapes. In the case of

[5]The spinning frequency f_{drop} of a micrometric MF drop can be estimated balancing the tangential magnetic stress and the viscous stress at the drop boundary [21] $F_{\mathrm{drop}} \approx f\frac{\mu_0}{4}\frac{V_p}{k_B T}\frac{\eta}{\eta_0}\chi H_0^2$, where f is the magnetic field frequency and V_p is the mean magnetic particle volume. This simple estimate gives the observed order of magnitude for f_{drop}: $f_{\mathrm{drop}} \sim 0.1\, f$ for $H_0 = 300\,\mathrm{A\,m^{-1}}$.

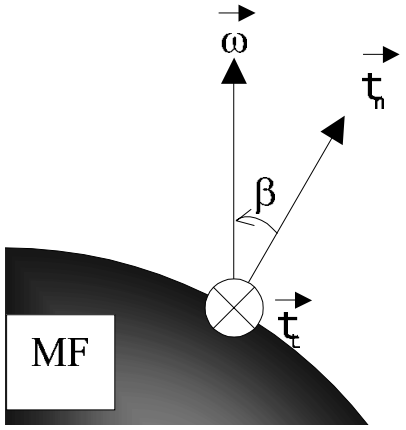

Fig. 9. Normal stress $\boldsymbol{t}_n$ and tangential stress $\boldsymbol{t}_t$ at the curved surface of a MF submitted to a rotating magnetic field. $\boldsymbol{\omega}$ is the rotation vector of the field and β is the angle between $\boldsymbol{\omega}$ and the normal to the surface.

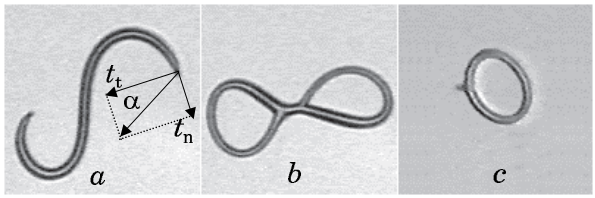

Fig. 10. (a) Tangential and normal stresses at the ends of a stretched drop. If $t_t >> t_n$, the drop tends to form loops and can adopt an "8" shape (b) or an "O" shape (c). Whereas the "S" and the "8" shape are usually unstable, the "O" (ring) shape can stay stable for several minutes.

more complex dynamic structures such as the intermediate shapes between the prolate ellipsoid and the star shape described in Fig. 4, the situation is more complicated, as discussed in the following section.

3.2. The "S" shape. Starting from the prolate ellipsoidal shape and increasing ω, the drop bends at the end and adopts an "S" shape, as shown in Figs. 6, 7, and 10. This transition results from the competition between the normal and tangential stress, as sketched in Fig. 10a. Let α be the angle between the total stress at the end of the drop and the tangential stress: $\tan\alpha = t_n/t_t = \mu_0 M_n^2/(4\xi\omega)$. If $t_n >> t_t$, $\alpha = \pi/2$: the force exerted at the drop end tends to stretch it in the direction of $\boldsymbol{t}_n$, i.e., in the direction of the drop elongation. This results in the prolate ellipsoid shape. But if $t_t >> t_n$, $\alpha = 0$: the drop end, submitted to a radial force, tends to describe a circle. As both drop ends are submitted to a force that bends them in the direction of rotation of the magnetic field, the drop adopts an "S" shape. This morphology is dynamic: it tends to evolve towards an "8" shape, where the two ends coalesce in the middle of the drop (Fig. 6b and 10b), or to an "O" shape which involves less curvature (Fig. 10c). But the drop does not always achieve this structure. The MF thread elastic constant is a complicated function of H_0 and ω. Depending on the external parameters, the MF drop may not be able to support an important curvature: it breaks into several smaller droplets, the breakage taking place in the regions of high curvature (for example in Fig. 7).[6]

[6]Some steady ring shapes (Fig. 10c) have been observed in the experiments. Such a shape rarely occurs, though it can stay stable during the time of observation, of the order of several minutes.

3.3. The oblate–prolate transition. At low frequency and magnetic field amplitude, the situation is nearly static at the macroscopic scale. We can try to understand the symmetry breaking from the initial spherical shape to the slender shape (Figs. 3 and 4) using an energetic argument, as presented in ref. [22]. Let us consider an ellipsoidal drop of volume V submitted to a rotating magnetic field ($H_x = H_0 \cos \omega t$, $H_y = H_0 \sin \omega t$) in the regime $\tau_C^{-1} << \omega << \tau_B^{-1}$ where τ_B is the Brownian relaxation time of the magnetic particles. For simplicity, let us assume that the shapes are ellipsoidal: for low H_0, the ellipsoid is oblate, and it turns into a prolate ellipsoid when H_0 increases. These simple shapes are compatible with experimental observation. Under this assumption, the droplet magnetization is spatially homogeneous inside the drop: it depends only on the external parameters and on the ellipsoid aspect ratio.

In the case of a prolate ellipsoid, the magnetization is not strictly perpendicular to the ellipsoid long axis, but it has two perpendicular components along the two principal axis in the plane of the rotating field. The drop magnetic energy is then the sum of two contributions:

$$E_{\mathrm{MP}} = -\frac{1}{2}\mu_0 V \chi H_0^2 \Big(\frac{\cos^2 \omega t}{1 + n_1 \chi} + \frac{\sin^2 \omega t}{1 + n_2 \chi} \Big), \tag{5}$$

where n_1 and n_2 are two demagnetizing factors respectively along the ellipsoid long axis and along the ellipsoid small axis [22]. n_1 and n_2 depend only on the ellipsoid aspect ratio.

In the case of an oblate ellipsoid, after averaging the orientation of the rotating magnetic field, the magnetic energy is

$$E_{\mathrm{MO}} = -\frac{1}{2}\mu_0 V \chi H_0^2 \frac{1}{1 + n_0 \chi}, \tag{6}$$

where n_0 is the demagnetizing factor of the oblate ellipsoid in the plane of rotation of the magnetic field [22].

The total energy of the drop contains the magnetic and the interfacial energy contributions. Minimization of the total energy versus the ellipsoid large to small length ratio K leads to the equilibrium shape for the prolate and the oblate shape. The shape is a function of H_0: the higher H_0, the higher K. The results of the energy minimization show that the energy minimum is smaller for the oblate shape than for the prolate one for very low H_0, while $K_{\mathrm{O}} < 1.3$ (here, the subscript O stands for "oblate" and the subscript P for "prolate"). For larger value of H_0, corresponding to an ellipsoid aspect ratio $K_{\mathrm{P}} \sim 10$, the prolate shape becomes energetically more favorable. A transition from an oblate shape $K_{\mathrm{O}} \sim 1.3$ to a prolate one $K_{\mathrm{P}} \sim 10$ is actually experimentally observed at low frequency (4 Hz to 1 kHz) when increasing H_0 (see the first two images of each sequence of Fig. 3*a* to 3*d*).

A more detailed computation [22] shows that for higher frequencies and for high values of H_0, the oblate shape is more stable, as observed experimentally. This calculation is based on the equation of motion of magnetic particles in a rotating magnetic field, both in the case of an oblate shape and of a prolate shape.

For higher frequencies (f = 4 kHz), the spinning effects become more important and the drop does not elongate for small values of H_0 (see Fig. 3*e*). The limit of the model is reached and the static description is not valid anymore.

3.4. The magnetic fluid starfish. The MF starfish shape is due to the magnetic normal surface stress (Eq. (3)). Why do peaks appear at the edge of the disk and why does the number of peaks increase with the magnetic field? This phenomenon is analogous to peak formation at the free surface of a MF submitted to a perpendicular magnetic field, and is known as the normal field instability [1]. Our experiments are performed in the regime $\omega \tau_C >> 1$. The orientation of the rotating magnetic field must thus be time-averaged: each point of the droplet interface experiments a radial magnetic field. Let us consider a cylindrical MF drop whose circular section is in the plane of rotation of the external magnetic field. If a perturbation (a thermal fluctuation for instance) $\zeta = \zeta_0 \exp[i(\Omega t - \mathbf{k}.\mathbf{r})]$ propagates at the drop interface perpendicularly to the cylinder axis, it has been shown

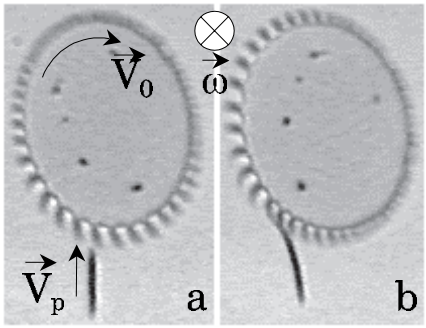

Fig. 11. Interaction between two MF droplets of different volume, submitted to a clockwise rotating external magnetic field. A small prolate droplet (in the bottom of the figure) is attracted by a bigger oblate drop rotating clockwise at the velocity $V_{\rm O}$. (a) $t = 0$: the prolate droplet (velocity $V_{\rm P}$) moves straight towards the center of gravity of the oblate drop, showing that magnetic interaction is dominant. (b) t = 0.20 s: the prolate drop touches the spikes of the oblate drop and is swept along by the drop spinning motion. The two drops then merge in a single oblate ellipsoidal drop rotating clockwise.

in ref. [18, 22] that the dispersion relationship is

$$\rho\Omega^2 = \sigma k\frac{a^2\,k^2-1}{a^2} - 2\mu_0 H_0^2\frac{\chi^3}{(\chi+2)^3}k\frac{ak-1}{a}, \tag{7}$$

where a is the cylindrical drop radius. The first term on the right side of Eq. (7) is the surface tension stabilizing term. The last term is the magnetic destabilizing term: when $\Omega^2 < 0$, the amplitude of the perturbation grows exponentially and instability develops, leading to the formation of peaks at the interface. Since $ka > 1$, the interface is always unstable for small k. For an infinite surface, the most unstable wave vector scales as $k \sim \mu_0 H_0^2/\sigma$. For a confined geometry (a finite MF volume), the wave vector is quantified by the drop radius: the possible values of the wave vector are $k_n = 2\pi n/a$, where n is the number of peaks. Therefore, n scales as H_0^2. Experiments and theory are in good agreement whatever the rotating field frequency, as shown in ref. [18].

3.5. Interaction between droplets. The presented experiment usually involves a number of droplets in motion, which are in interaction via magnetic interaction or hydrodynamic interaction. Magnetic interactions are on average attractive in the plane of rotation of the external magnetic field, and droplet coalescence is observed. Figure 11 shows such a collapse between two MF drops submitted to a rotating magnetic field. As the drop morphology depends on its size, the big droplet has a spiny oblate shape whereas the small one is a prolate ellipsoid. When the two droplets are far enough, they both rotate in the same direction as the external field, with a frequency that depends on its size. As they come closer to one another, the small prolate drop slows down its spinning motion. Its velocity becomes linear, directed towards the center of gravity of the oblate drop, as shown in Fig. 11a. At this stage, its motion is dominated by magnetic interaction, which is a central force. In Fig. 11b, the prolate droplet comes into contact with the other drop and is dragged by the spinning motion of the prolate drop. After a few seconds, the two drops end up coalescing in a bigger spiny oblate ellipsoid rotating clockwise. This experiment shows that the prolate drop trajectory does not deviate from a straight line until it comes into contact with the oblate drop. This suggests that the hydrodynamic radius of the spinning oblate drop is not different from the drop radius.

Conclusions

We have observed the behavior of a MF microdrop in a rotating magnetic field as a function of the field intensity and frequency. The observed patterns and dynamics are very rich; they are all attributed to the surface

effect of a MF interface submitted to a rotating magnetic field. Shape and motion of the MF drop can be understood separately. On the one hand, the competition between the magnetic normal stress and the surface tension is responsible for the drop radial extension. On the other hand, the drop rotation motion is due to the competition between the tangential frequency dependent stress and the drop viscous torque.

REFERENCES

1. R. E. ROSENSWEIG. *Ferrohydrodynamics* (Cambridge University Press, New York, 1985).
2. E. BLUMS, A. O. CEBERS, AND M. M. MAIOROV. *Magnetic Fluids* (de Gruyter, Berlin, New York 1997).
3. Labyrinthine Pattern Formation in Magnetic Liquids. Special issue of *Magnetohydrodynamics*, vol. 35 (1999).
4. R. MOSKOWITZ AND R. E. ROSENSWEIG. *Appl. Phys. Lett.*, vol. 11 (1967), p. 301.
5. R. BROWN AND T. S. HORSNELL. *Electr. Rev.*, (1969), p. 235.
6. R. MAILFERT AND A. MARTINET. Macro-organized patterns in ferrofluid layer: Experimental studies. *J. Phys.*, vol. 34 (1973), p. 197.
7. R. E. ROSENSWEIG, J. POPPLEWELL, AND R. J. JOHNSTON. *J. Mag Mag Mat*, vol. 85 (1990), p. 171.
8. A. V. LEBEDEV AND A. F. PSHENICHNIKOV. *Magn. Gidrod.*, vol. 1 (1991), p. 7.
9. J.-C. BACRI, D. SALIN , R. PERZYNSKI, V. CABUIL, AND R. MASSART. In *J. Colloid Interface Sci.* , vol. 132 (1989), p. 43.
10. E. DUBOIS, R. PERZYNSKI, F. BOUÉ, AND V. CABUIL. *Langmuir*, vol. 16 (2000), p. 5617.
11. J.-C. BACRI AND D. SALIN *J. Phys. Lett.*, vol. 43 (1982), p. L179.
12. J.-C. BACRI AND D. SALIN. *J. Phys. Lett.*, vol. 43 (1982), p. L649.
13. J.-C. BACRI AND D. SALIN. *J. Phys. Lett.*, vol. 44 (1983), p. L415.
14. O. SANDRE, J. BROWAEYS, R. PERZYNSKI, J.-C. BACRI, V. CABUIL, AND R. E. ROSENSWEIG. *Phys. Rev. E*, vol. 59 (1999), p. 1736.
15. G. HELGESESN, P. PIERANSKI, AND A. T. SKJELTROP. *Phys. Rev. Lett.*, vol. 64 (1990), p. 1425.
    P. PIERANSKI, S. CLAUSEN, G. P. HELGESEN, AND A. T. SKJELTROP. *, Phys. Rev. Lett.* , vol. 77 (1996), p. 1620.
    S. CLAUSEN, G. P. HELGESEN, AND A. T. SKJELTROP. *Phys. Rev. E*, vol. 58 (1998), p. 4229.
16. D. REGUERA, J. M. RUBÍ, AND A. PÉREZ-MADRID. *Phys. Rev. E* , vol. 62 (2000), no. 5313, pp. 2460–2463.
17. J.-C. BACRI, R. PERZYNSKI, D. SALIN, AND A. O. CEBERS. *Mat. Res. Soc. Symp. Proc.*, vol. 248 (1992), p. 241.
18. J.-C. BACRI, A. O. CEBERS, AND R. PERZYNSKI. *Phys. Rev. Lett.,* , vol. 72 (1994), p. 2705.
19. O. SANDRE. (private communication).
20. J.-C. BACRI, R. PERZYNSKI, M. I. SHLIOMIS, AND G. I. BURDE. *Phys. Rev. Lett*, vol. 75 (1995), p. 2128.
21. A. O. CEBERS. *Magnetohydrodynamics*, vol. 11 (1975), pp. 63–65.
22. A. CEBERS AND S. LACIS. *Brazilian Journal of Physics*, vol. 25 (1995), p. 101.